Electronic Supplementary Information (ESI)

A synergy between ultrasonication and polymer matrix in reducing particle size of molecular explosive during crystallization

Soojin Lee, Jumi Lee, Kuktae Kwon, Eunhee Ko, Eunji Lee,
Chung-Jong Yu, Kwanwoo Shin, and Jungwook Kim

1. Experimental Section

1.1. Materials

RDX and polyacrylate elastomer HyTemp (4454, Zeon Chemicals) were obtained from Agency for Defense Development (Republic of Korea). γ-Butyrolactone (GBL) was purchased from Tokyo Chemical Industry. Distilled water and ethanol were purchased from Daejung Chemicals. All materials were used as-received.

1.2. Characterization of crystalline RDX particles

RDX samples crystallized from various methods (with or without ultrasonication and/or polymer matrix) were imaged by a field emission scanning electron microscope (FE-SEM, Inspect F, FEI). Elemental analysis of the samples was conducted using an energy dispersive X-ray spectroscope (EDS, Apollo X, EDAX) equipped in FE-SEM. For RDX crystallized inside HyTemp, the samples were cleaved inside liquid nitrogen and sputtered with Pt for cross-sectional imaging by FE-SEM. RDX samples crystallized inside HyTemp were also imaged by a transmission electron microscopy (JEM-1400, JEOL or Bio-TEM, Tecnai G2 Spirit Twin, FEI). Samples were sectioned to either 60 nm or 100 nm thicknesses at – 60 °C with a cryo-ultramicrotome (EMFC7, LEICA). Sectioned samples were deposited on carbon coated grids and stained using either 2 % ruthenium tetroxide or 2 % osmium tetroxide solution (Electron Microscopy Science). The grids were then coated with or without 2 % methylcellulose solution (Sigma-Aldrich) and imaged by TEM.

HyTemp, as-received RDX, and RDX crystallized inside HyTemp were examined by X-ray scattering and thermoanalytical methods. A Rigaku rotating anode CuKa (l = 0.1541 nm) X-ray source operating at 40 kV -30 mA were used to perform small angle X-ray scattering (SAXS) and X-ray diffraction (XRD) measurements. The sample-to-detector distances for SAXS and XRD were 1.4 m and 0.17 m respectively. Scattering intensities were collected on a two-dimension area detector for 20 min and then circularly averaged. All samples were measured at room temperature. For thermal analysis using a differential scanning calorimeter (DSC, DSC-Q20, TA Instrument), samples were placed in an aluminum pan with a pin-hole cover, and heated from 40 °C to 250 °C at a constant heating rate of 5 °C·min^{-1} under nitrogen atmosphere. To minimize the effect of the sample size on measured melting temperature, all samples had similar weight (1.3 – 1.5 mg) of

RDX and weight fraction of RDX inside the polymer matrix (32 – 36 wt %). For thermal analysis using a thermogravimetric analyzer (TGA, TGA-Q50, TA Instruments), samples were examined at a constant heating rate of 10 °C·min^{-1} in the temperature range of 40 – 500 °C under a dynamic nitrogen flow rate of 40 ml·min^{-1}.

1.3. Measurements of the solubility and an equilibrium partition coefficient of RDX inside HyTemp

The solubility of RDX in GBL at the pre-crystallization and crystallization temperatures, 68 °C and – 35 °C, respectively, was measured by dissolving an excess amount of RDX in GBL at each temperature for several days and carefully withdrawing the supernatant solution. The supernatant solution withdrawn at 68 °C was diluted below the saturated concentration at room temperature. The concentration of the supernatant solution was measured by UV-Vis spectrophotometer (Cary 100, Agilent) using the solutions with known RDX concentrations as the reference materials. To check the validity of our solubility measurement, we compared the experimentally measured solubility to the theoretical one predicted by the Schröder−van Laar equation

$$x = \frac{1}{\gamma} exp\left(\frac{\Delta H_f}{R}\left(\frac{1}{T_m} - \frac{1}{T}\right)\right) \quad (1)$$

where x, γ, R, ΔH_f, and T_m are the mole fraction and activity coefficient of RDX in GBL at a temperature T, gas constant, and enthalpy of fusion and melting temperature of RDX, respectively. To predict γ at the pre-crystallization and crystallization temperatures, we used a simple function γ(T) = a·exp(b/T) to fit the calculated values of γ at temperatures at which x is reported,[2] although the theoretical estimation of γ is a much more complicated function of both temperature and mole fraction.[3] The predicted form of γ(T) was substituted into the Schröder−van Laar equation, which is drawn in Figure S4.

An equilibrium partition coefficient of RDX was measured at 65 °C and – 35 °C and as the ratio of the concentration of RDX in the GBL solution absorbed inside HyTemp to that in the outside bulk solution at an equilibrium condition at each temperature. Briefly, a 200 mg of RDX was dissolved in a 1 mL of GBL in the microtube at room temperature, to which a 50 mg of HyTemp was added. The microtube was then placed in the temperature-controlled shaking incubator maintained at 68 °C for 18 hours to obtain an equilibrium partitioning of RDX inside HyTemp at each temperature. After a careful removal of HyTemp swollen by the GBL solution of RDX, a volume, mass, and RDX concentration of the remaining solution were measured. Using measured values and a density of GBL, a mass of RDX and a volume of GBL in the remaining solution and also those inside HyTemp were calculated, from which the concentration of RDX in the GBL solution absorbed by HyTemp was calculated. To measure the equilibrium partition coefficient at – 35 °C, we used the same protocol except: a 20 mg of RDX is dissolved in a 1 mL of GBL

containing a 50 mg of HyTemp and the microtube was placed in the immersion bath maintained at – 35 °C for 18 hours.

2. Interaction between RDX and polymer matrix

We examine whether the interaction between RDX and polymer matrix is favorable such that nucleation can be expedited. From the classical nucleation theory, the rate of heterogeneous nucleation is expressed as[4]

$$J = A \cdot exp\left[-\frac{16\pi\gamma^3 v^2 \ f(\theta)}{3k_B^3 T^2 \ (lnS)^2} \right] \quad (2)$$

where A is the prefactor determined from kinetic considerations and is proportional to the number density of nucleation site and the rate of molecular transport and attachment to nucleus. γ, v, k_B, T and S represent the nucleus-solvent interfacial energy density, volume of a single solute molecule, Boltzmann constant, temperature, and supersaturation, respectively. $f(\theta)$ represents a reduction of the free energy barrier for nucleation due to a pre-existing surface and is an increasing function of θ, which is the contact angle made at the interface between the nucleus, solvent, and surface (here, the polymer matrix). Thus, θ is an indirect measure of a quality of interaction between the nucleus and surface in the presence of solvent. θ can be estimated by the Young's equation; however, a calculation of the interfacial energy density at the temperature of interest requires the dispersive and polar components of the surface energy density, γ^d and γ^p, respectively, for each material at that temperature.[5] Although γ^d and γ^p relevant to room temperature are either reported for RDX and HyTemp[6] or can be calculated for GBL using the empirical equation with solubility parameters as variables,[7] γ^d and γ^p relevant to the crystallization temperature (– 35 °C) are practically hard to estimate or measure.

Instead, we measure the equilibrium partition coefficient of RDX, which is defined here as the equilibrium ratio of the RDX mass fraction in the GBL solution between inside and outside the polymer matrix. The measured equilibrium partition coefficient is related to chemical potentials of RDX in the GBL solution inside and outside the polymer matrix, and chemical potentials can be expressed using the Flory-Huggins and the Flory-Rehner equations with parameters such as the molecular weight of polymer segment between crosslinks, volume fraction of each species, and Flory-Huggins interaction parameter.[8] Therefore, if the parameters are known, one can calculate the contact angle from the equilibrium partition coefficient. Here, the measured equilibrium partition coefficient of RDX is almost one at the crystallization temperature (– 35 °C), as summarized in Table S1. Such condition indicates that the polymer matrix has no energetic preference for RDX over GBL or *vice versa*.[9] Therefore, without needing to know the parameters to calculate chemical potentials, we get $\gamma_{pn} \approx \gamma_{ps}$ where the subscript *p*, *n*, and *s* indicate the polymer matrix, nucleus (RDX), and solvent, respectively. From the Young's equation, we get $\theta \approx \pi/2$, and

for a smooth surface, $f(\theta)$ is estimated to be $^{1/2 - 3\cos(\theta)/4 + \cos^3(\theta)/4}$ [10] such that $f(\pi/2) \approx 0.5$. Consequently, heterogeneous nucleation by itself may increase the rate of nucleation of RDX in HyTemp.

However, the polymer matrix has adverse effects as well on expediting nucleation. Supersaturation, defined as the ratio of the RDX concentration between the pre-crystallization and crystallization temperatures, is reduced from 11.7 for quenching the bulks solution (Q) to 9.4 for quenching the solution inside the polymer matrix (QM), as summarized in Table S1. Substituting measured supersaturation and $f(\theta)$ into the equation 1, we find that the rate of heterogeneous nucleation is faster than the rate of homogeneous nucleation for a constant value of the prefactor A. However, as a transport of RDX molecules is retarded inside the polymer matrix due to steric obstruction and/or hydrodynamic drag by the polymer matrix[9] and also the number density of nucleation site is altered, the prefactor A should vary between homogeneous and heterogeneous nucleation. Overall, given that RDX particles obtained by QM is roughly an order of magnitude smaller than those achieved by quenching only, we infer that the effects of heterogeneous nucleation are greater than those of reduced supersaturation and retarded molecular transport.

Table S1. Solubility of RDX in GBL for the bulk solution and solution inside the polymer matrix and calculated supersaturation and partition coefficient.

		65 °C	-35 °C	Supersaturation
RDX solubility in GBL (mg/ml)	Bulk solution	363	31	11.7
	Solution in matrix	287	30	9.4
Partition coefficient		0.79	0.99	

Table S2. Atomic fractions (%) of carbon, nitrogen, and oxygen detected by EDS for the polymer matrix, RDX, and polymer matrix embedded with RDX crystallized by QUM. Standard deviations are calculated from independent measurement of five polymer matrix with embedded RDX.

	C	N	O
HyTemp	79.9	0.0	20.1
RDX	34.8	33.3	32.0

RDX in HyTemp	65.2 ± 5.8	17.0 ± 6.4	17.8 ± 3.8

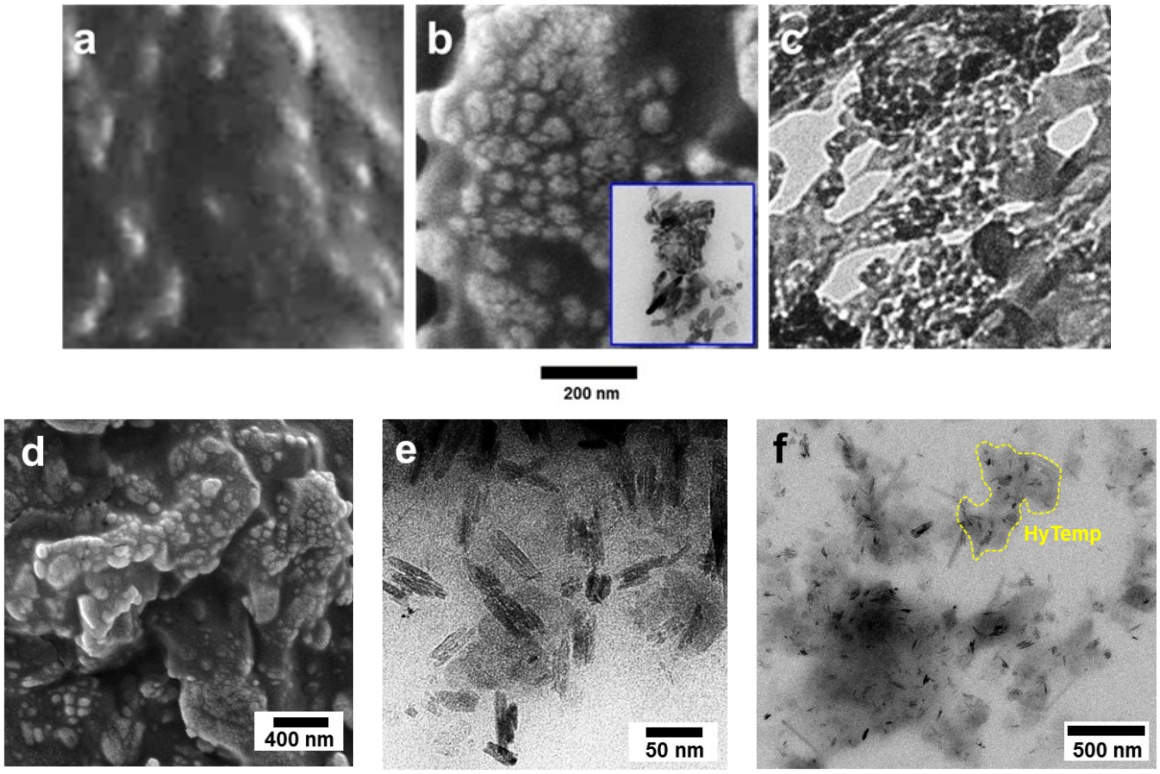

Figure S1. SEM (a, b, d) and TEM (inset of b, c, e, f) images of RDX crystallized by QUM. For a, b (including the inset), and c, the same scale bar of 200 nm is applied. Note that dot-like protrusions have similar length scale, which is a few tens of nanometers.

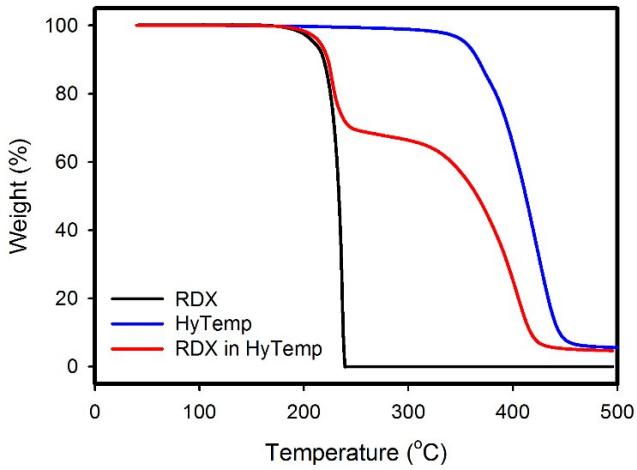

Figure S2. TGA spectra of the polymer matrix, RDX, and polymer matrix embedded with RDX particles crystallized by QUM. The calculated weight fraction of RDX inside the polymer matrix is approximately 33 - 36 wt. %. A residual mass fraction of approximately 5 wt. % upon a complete

decomposition of polymer matrix above 450 °C is due to amorphous silica initially contained in the HyTemp elastomer, which is 1 – 5 wt. % as reported by the manufacturer.

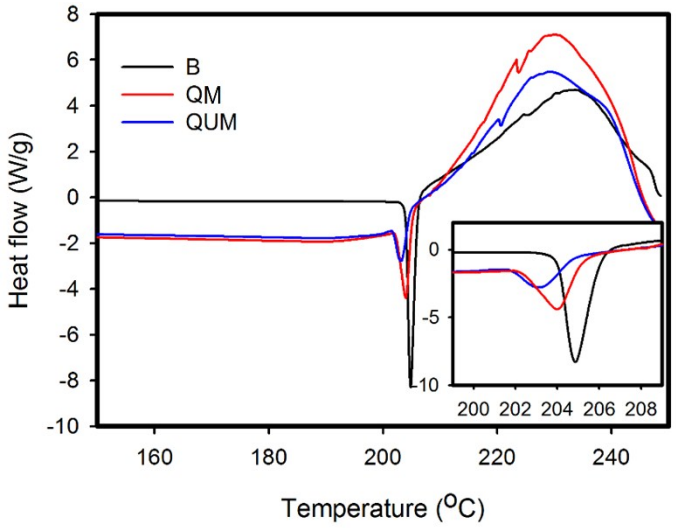

Figure S3. DSC spectra of bulk RDX (B), RDX nanoparticles crystallized inside the polymer matrix by QM or QUM. All samples have approximately 1.3 – 1.5 mg of RDX, and the weight fractions of RDX for QM and QUM samples are 32 – 36 wt. % (rests are the polymer matrix). While a broad exothermic peak corresponding to RDX decomposition is similar in magnitude between samples, a sharp endothermic peak around 203 – 205 °C corresponding to RDX melting is varied in the peak temperature as well as magnitude between samples (inset). We infer that a large reduction in magnitude of the endothermic peak from B sample to QUM (or QM) sample is due primarily to an onset of decomposition prior to melting for QUM (or QM) sample, as indicated by a slight increase in the heat flow before melting. As thermal energy generated by initial decomposition is partially absorbed during melting, the amount of thermal energy supplied to QUM (or QM) sample by DSC is reduced, which lowers magnitude of the endothermic peak. An earlier onset of decomposition has been reported by previous studies, which demonstrate that the activation energy of RDX for decomposition is reduced inside the polymer matrix.[11] For the estimation of the particle size, we used the Gibbs-Thomson equation, $T_{mB} - T_m = (4T_{mB}\gamma_{sl})/(\Delta H_f \rho_s x)$ where T_{mB}, T_m, γ_{sl}, ΔH_f, and ρ_s represent melting temperatures of a bulk crystal and a small crystal of size x, solid-liquid interfacial energy density, enthalpy of fusion, and density of solid crystal, respectively. The enthalpy of fusion and the density of RDX reported previously,[3] which are respectively 35,648 J/mol and 1.82 g/cm^3. For estimating the particle size using the Gibbs-Thomson equation, we assume that a thin layer of the RDX solution surrounds the particle[12] and resulting γ_{sl} of RDX is around 5 – 20 dyn·cm^{-1}, which is the estimated values from molecules with comparable size and chemistry to RDX.[13]

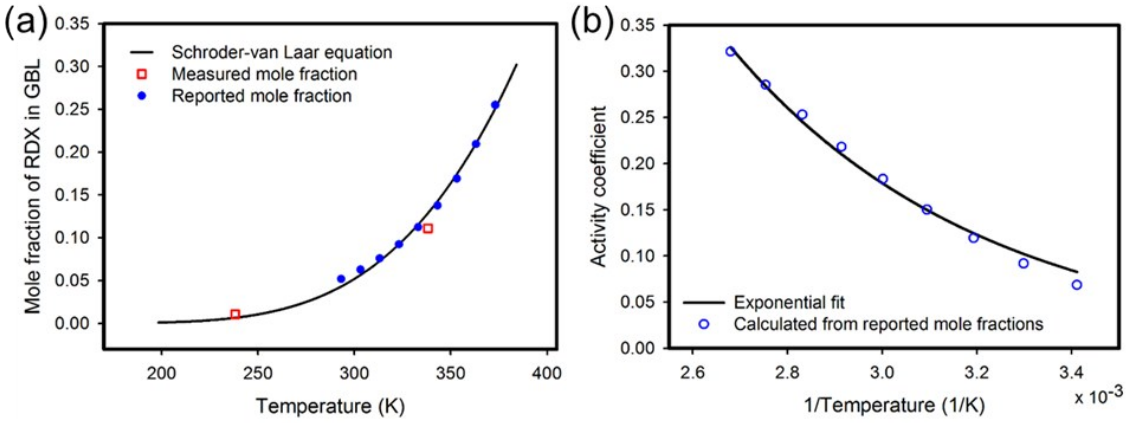

Figure S4. (a) The measured solubility of RDX in GBL at the pre-crystallization and crystallization temperatures (red squares) is compared to the theoretical solubility (a solid line) predicted by the Schröder−van Laar equation. The value of γ at temperatures at which x is reported (blue circles) is calculated using the Schröder−van Laar equation. (b) The calculated values of γ are fitted to a simple exponential function, from which values of γ at the pre-crystallization and crystallization temperatures are estimated.

References

1. A. Wuillaume, A. Beaucamp, F. David-Quillot and C. Eradès, *Propellants Explos. Pyrotech.*, 2014, **39**, 390.
2. J.-W. Kim, J.-K. Kim, H.-S. Kim and K.-K. Koo, *Organic Process Research & Development*, 2011, **15**, 602.
3. J. E. Lee, J. W. Kim, S. K. Han, J. S. Chae, K. D. Lee and K. K. Koo, *Ind. Eng. Chem. Res.*, 2014, **53**, 4739.
4. S. Karthika, T. K. Radhakrishnan and P. Kalaichelvi, *Crystal Growth & Design*, 2016, **16**, 6663.
5. L. A. Girifalco and R. J. Good, *The Journal of Physical Chemistry*, 1957, **61**, 904.
6. J. S. Shim, H. S. Kim, K. D. Lee and J. K. Kim, 2004 Annual Conference of AIChE, 2004.
7. M. Belmares, M. Blanco, W. A. Goddard, R. B. Ross, G. Caldwell, S. H. Chou, J. Pham, P. M. Olofson and C. Thomas, *J. Comput. Chem.*, 2004, **25**, 1814.
8. A. Ahmad, A. J. Tinker and D. W. Aubrey, *Journal of Natural Rubber Research*, 1995, **10**, 1.
9. T. J. Dursch, N. O. Taylor, D. E. Liu, R. Y. Wu, J. M. Prausnitz and C. J. Radke, *Biomaterials*, 2014, **35**, 620.
10. P. S. Richard, *J. Phys.: Condens. Matter*, 2007, **19**, 033101.
11. F. Pessina, F. Schnell and D. Spitzer, *Chem. Eng. J.*, 2016, **291**, 12.
12. S. L. Lai, J. Y. Guo, V. Petrova, G. Ramanath and L. H. Allen, Phys. Rev. Lett., 1996, 77, 99.
13. O. Yavuz, A. Sezen, K. Kazım and M. Necmettin, J. Phys. D: Appl. Phys., 2008, 41, 065309.